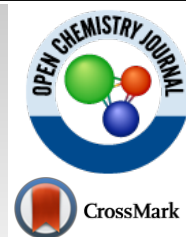




# Open Chemistry Journal

Content list available at: <https://openchemistryjournal.com>



## RESEARCH ARTICLE

### Preparation of $\text{PbI}_2$ Microflakes by pH-Controlled Double-Jet Precipitation

Haifang Huang<sup>1</sup>, Xing Chen<sup>1</sup> and Kai Huang<sup>1,2,\*</sup>

<sup>1</sup>School of Metallurgical and Ecological Engineering, University of Science and Technology Beijing, Xueyuan Rd.30, Haidian District, 100083, Beijing, China

<sup>2</sup>Beijing Key Lab of Green Recycling and Extraction of Metals, University of Science and Technology Beijing, Xueyuan Rd.30, Haidian District, 100083, Beijing, China

#### Abstract:

#### Introduction:

Pure  $\text{PbI}_2$  crystal particles with a flaky shape were prepared by a pH-constant double-jet precipitation process, which has the significant advantages of easy operation and scaling-up. It was found that a pH below 5.0 of the mixing solution is the appropriate range for the formation of pure  $\text{PbI}_2$  phase, while at a pH above 5.0, the  $\text{PbIOH}$  phase would appear immediately and decrease its solubility in DMF (dimethylformamide) for the preparation of a high-quality film of perovskite solar cells.

#### Materials and Methods:

Various instruments, including XRD, FTIR, SEM/EDS were used to characterize the precipitated particles obtained under different experimental conditions, and the effect of various parameters, including pH, concentration of the lead ions, feeding rate, and the characteristics of the surfactants on the particle was investigated systematically. Thermodynamic calculation of species distribution in the solution systems of  $\text{Pb}^{2+}$ -I- $\text{H}_2\text{O}$ ,  $\text{Pb}^{2+}$ -I-Cit- $\text{H}_2\text{O}$  and  $\text{Pb}^{2+}$ -I-EDTA- $\text{H}_2\text{O}$  were carried out to identify the indispensable role of pH on the formation of highly pure lead iodide crystals. The crystallization of  $\text{PbI}_2$  was regarded as the basis of the formation of flake-like products, which was also strongly dependent on the pH value of the solution.

#### Results:

It was found that at a low concentration of the  $\text{PbI}_2$  precursor, such as with very dilute lead ions or with a very slow feeding rate, the XRD reflection peaks at  $12.67^\circ$ ,  $38.67^\circ$  and  $52.39^\circ$  will dominate, while the peaks at  $25.91^\circ$ ,  $34.27^\circ$ , and  $39.51^\circ$  will become dominant in the case of high concentration. The lead iodide particles were tested by mixing them in DMF, and it was found that the samples precipitated at a pH of 2 and 4 could dissolve and form a homogeneous solution easily, while the sample produced at a pH of 6 would form a turbid suspension, and could not dissolve completely to obtain a clear solution.

#### Conclusion:

The results presented in this work provide detailed and significant information about the synthesis of highly pure  $\text{PbI}_2$ , which may be applied in the fabrication of perovskite solar cells.

**Keywords:** Lead iodide, Constant pH, Double-jet precipitation, Morphological evolution, XRD, FTIR.

#### Article History

Received: July 11, 2019

Revised: September 26, 2019

Accepted: October 06, 2019

## 1. INTRODUCTION

In recent years, lead iodide has caused many concerns in the scientific and industrial fields, because it is one of the ess-

\* Address correspondence to this author at School of Metallurgical and Ecological Engineering, University of Science and Technology Beijing, Xueyuan Rd.30, Haidian District, 100083, Beijing, China, Beijing Key Lab of Green Recycling and Extraction of Metals, University of Science and Technology Beijing, Xueyuan Rd.30, Haidian District, 100083, Beijing, China; Tel: +86-10-13552537538; E-mail: [khuang@metall.ustb.edu.cn](mailto:khuang@metall.ustb.edu.cn)

ential functional materials with extensive applications in the fabrication of detectors [1 - 6], co-precipitation sensors [7, 8], lasers [9 - 15], perovskite solar cells [16 - 22], active matrix flat panel imagers [23], and X-ray imaging [24 - 26]. Especially owing to its excellent photoelectronic transferring properties in perovskite solar cells, the study on the preparation of lead iodide has been carried out intensively [27, 28]. Among the above-mentioned applications, perovskite solar cells have drawn major attention due to their high power conversion

efficiency from solar light to electrical current, which has currently exceeded 22% [29 - 31]. Three major methods were designed to make perovskite solar cell film materials, including the solution method [32], the vacuum deposition method [33, 34] and the gas phase assisted solution method [35]. The most widely adopted preparation method is the solution process in which lead iodide and methylammonium iodide are dissolved in DMF in order to form a homogeneous solution, which is then used to prepare the film by spin coating or dripping. Considering that lead iodide is a particularly important basic raw material in the fabrication of perovskite solar cells, its purity, composition and degree of crystallization will influence its solubility in DMF, which is used as the solvent, as well as the quality of the fabricated perovskite solar cell film. Therefore, whether lead iodide can completely dissolve in DMF is inextricably linked to its purity. Therefore, its preparation method is quite important as it may directly influence the photoelectric transferring performance of the perovskite solar cell film. According to the literature [36, 37], the chemical composition and purity of lead iodide should be carefully controlled in its synthetic processes.

There are many methods to synthesize lead iodide particles, such as the lead iodide single crystal synthesis technique [38, 39], chemical precipitation, and the recrystallization method [40]. Although these methods have been reported, a systematic study on the relationship between the purity of lead iodide and its solubility in DMF is seldom mentioned. The present work provides a controlled method for the synthesis of lead iodide, and the synthesis parameters of the morphology and chemical compositions of lead iodide products are systematically studied, including pH, the concentration of lead ions, feeding rate, and surfactants. This study provides insights into how to control the purity and composition of lead iodide, as well as its solubility in DMF, which is crucial for the preparation of high-quality perovskite cells.

## 2. EXPERIMENTAL

### 2.1. Materials and Instruments

Lead nitrate (99.0%, Sinopharm Chemical Reagent Co., Ltd.), potassium iodide (99.0%, Tianjin Sailboat Chemical Reagent Technology Co., Ltd.), polyvinylpyrrolidone (99.0%, Shanghai Zhanyun Chemical Co., Ltd.), sodium citrate (99.0%, Beijing Chemical Works), EDTA (Beijing Chemical Works) and lead iodide as the standard sample (99.95%, Sinopharm Chemical Reagent Co., Ltd.) were acquired commercially and used without further purification. Experimental pH meter (PHSJ3F, Shanghai Jingke Technology Co., Ltd.), electronic balance (AUY220, Shimadzu Corporation, Japan), X-ray diffractometer (ZEISS, Germany), field emission scanning (ZEISS SUPRA55, Germany), energy dispersive spectrometer (OXFORD INCA X-ACT, America) and FT-Raman spectroscopy (8400S, Shimadzu Corporation, Japan) were used in this study.

### 2.2. Synthesis Procedure of $PbI_2$

The preparation of lead iodide in the present study is carried out through a pH-constantly controlled double-jet precipitation method. A schematic diagram of the synthesis procedure is shown in Fig. (1). In this typical synthesis procedure, 1.0 g (3 mmol) of  $Pb(NO_3)_2$  was dissolved in 100 ml of deionized water to prepare 0.03 mol/L  $Pb(NO_3)_2$  solution (solution A), and adjusted to pH=4 with  $HNO_3$ . At the same time, 1.1 g (6.6 mmol) of KI was dissolved in 100 ml of deionized water to prepare a 0.066 mol/L KI solution (solution B), which was adjusted to pH=4 with  $HNO_3$ . The next step was to measure 200 ml of deionized water (solution C), and adjust it to pH=4 with  $HNO_3$ . Then, solution A and solution B were added dropwise to solution C at a rate of 1 ml/min with the help of two peristaltic pumps, respectively. During the whole feeding process, the solution mixture was kept in a state of continuous stirring. When the feeding was completed with continuous stirring for 10 min, the supernatant liquid was filtered off. The lead iodide precipitate was then washed 3 times with deionized water of pH=4, and then the precipitate was collected and dried at 60 °C for 24 hours.

### 2.3. Characterization

In order to study the synthesized lead iodide powder, a series of analyses were conducted as follows. An X-ray diffractometer (ZEISS, Germany) with monochromatic  $CuK\alpha$  radiation ( $\lambda = 1.5406 \text{ \AA}$ ) at 40 kV and 50 mA was used to record the X-ray diffraction pattern of the lead iodide powder. The samples were scanned at a scanning rate of  $5^\circ \text{ min}^{-1}$  in the  $2\theta$  range of 10-90°. The appearance of the lead iodide powder was observed by using a scanning electron microscope, and the elemental composition characteristics of the powder were identified by an energy dispersive spectrometer (OXFORD INCA X-ACT, America). An FT-Raman spectroscopy instrument (Shimadzu Corporation, UV2600, Japan) was used to identify the functional groups of the lead iodide powder in the wavenumber range of 4000-500 nm.

## 3. RESULTS AND DISCUSSION

### 3.1. XRD

Sixteen samples were obtained under different conditions, and XRD was used to characterize these precipitated powders. Fig. (2) shows the XRD patterns of the lead iodide samples obtained at different pH values. It can be seen from Fig. (2) that the diffraction peaks of lead iodide powder prepared at pH=2 and 4 are in good agreement with the diffraction peak of standard  $PbI_2$ , which indicates that the purity of the sample was quite high. On the other hand, the diffraction peaks of lead iodide powder obtained at pH=6 also showed  $PbIOH$  as an impurity of lead iodide. Obviously, pH is a key factor for the chemical composition of the precipitated particles in the double jet precipitation process.

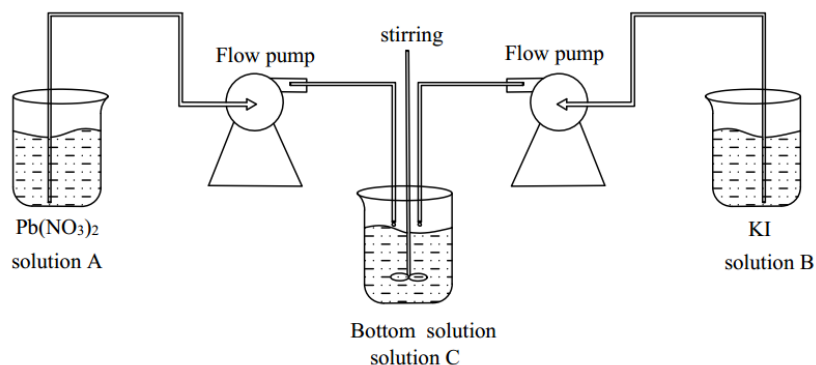


Fig. (1). The schematic diagram of the double-jet precipitation setup used for the preparation of lead iodide.

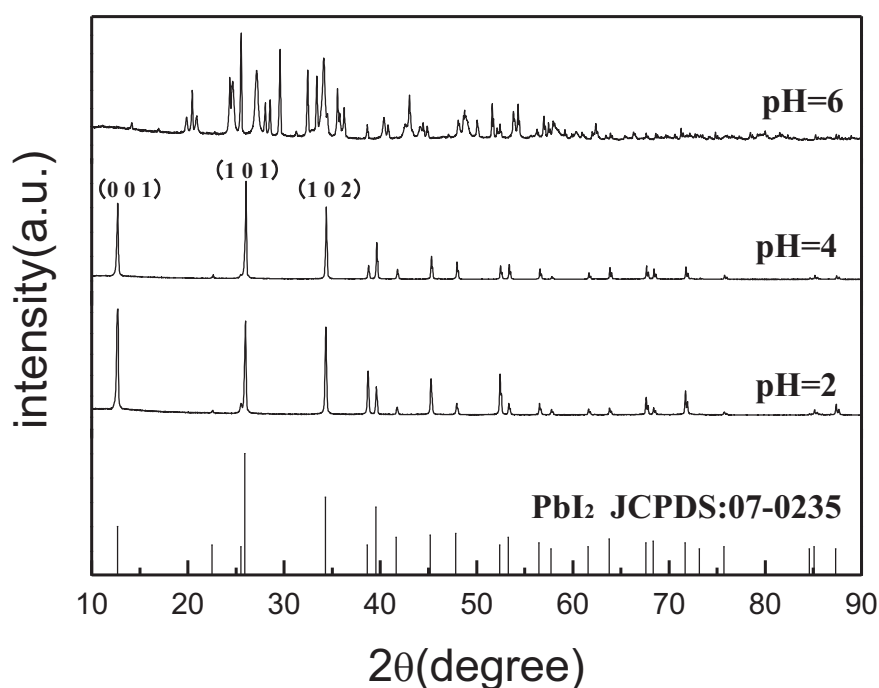


Fig. (2). XRD patterns of the  $\text{PbI}_2$  powders synthesized at different pH-values under the following experimental conditions:  $[\text{Pb(II)}]=0.03\text{mol/L}$ ,  $t=70\text{min}$ ,  $V=1.0\text{ml/min}$ .

Table 1. Thermodynamic data for the calculation of each species in the  $\text{Pb}^{2+}\text{-I}^- \text{-H}_2\text{O}$  aqueous solution.

S. No.	Relation	Constant
1	$\text{Pb}^{2+}2\text{I}^- = \text{PbI}_2$	$9.80 \times 10^{-9}$
2	$\text{Pb}^{2+}+2\text{OH}^- = \text{Pb(OH)}_2$	$1.43 \times 10^{-15}$
3	$\text{H}_2\text{O} = \text{H}^+ + \text{OH}^-$	$10^{-14}$

In order to learn more details about the aqueous solutions, the concentrations of lead and iodide species were calculated based on the mass balance of coordination between chemical species and thermodynamic constants of the  $\text{Pb}^{2+}\text{-I}^- \text{-H}_2\text{O}$  system as shown in Table 1. As demonstrated in Fig. (3), under acidic

conditions (pH 1~5),  $\text{Pb}^{2+}$ ,  $\text{PbI}^+$  and  $\text{PbI}_2$  are the dominant species, while at pH above 5.3,  $\text{PbIOH}$  would dominate as the only stable solid phase, which could be regarded as the mixing product of  $\text{PbI}$  and  $\text{Pb(OH)}_2$ . Both the experimental and calculated results were found to be identical in that they verify the important role of pH on the formation of pure lead iodide in the precipitation process. In the present study, the double jet precipitation process has a significant advantage of controlling the reaction pH very conveniently, which can avoid any pH fluctuation with an optimal range leading to the formation of  $\text{PbIOH}$ . On the basis of the above study, it could be concluded that the acidic pH condition determines the formation of pure  $\text{PbI}_2$  in the synthesis process that should be carefully controlled in the complete precipitation process.

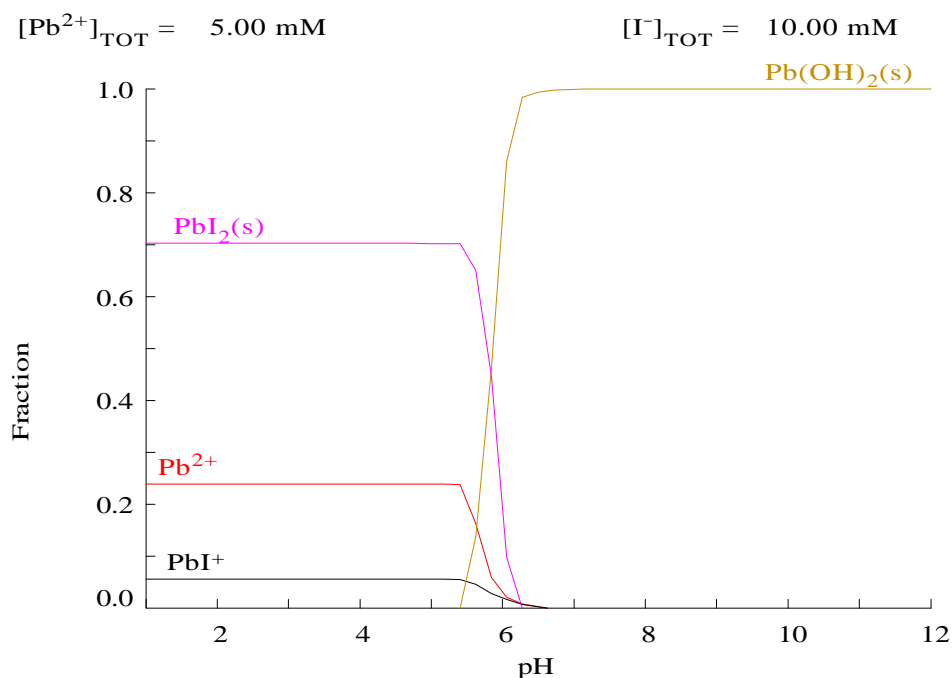


Fig. (3). Distribution species of  $\text{Pb}^{2+}$  and  $\text{I}^-$  in the  $\text{Pb}^{2+}$ - $\text{I}^-$ - $\text{H}_2\text{O}$  aqueous solution.

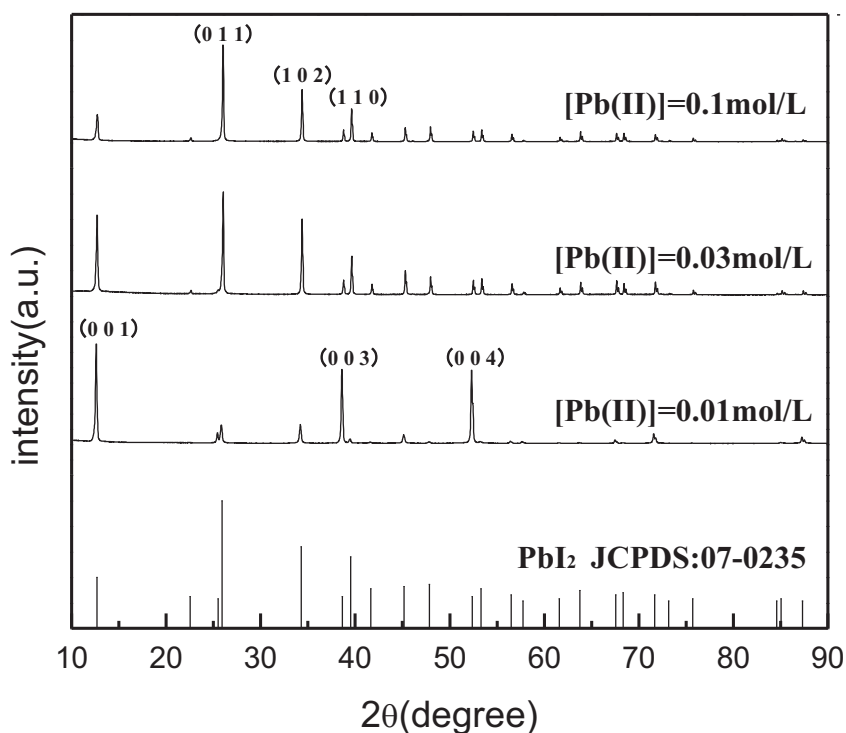


Fig. (4). XRD patterns of the  $\text{PbI}_2$  powders synthesized at different lead ion concentrations under the following experimental conditions:  $\text{pH}=4$ ,  $t=70\text{min}$ ,  $V=1.0\text{ml/min}$ .

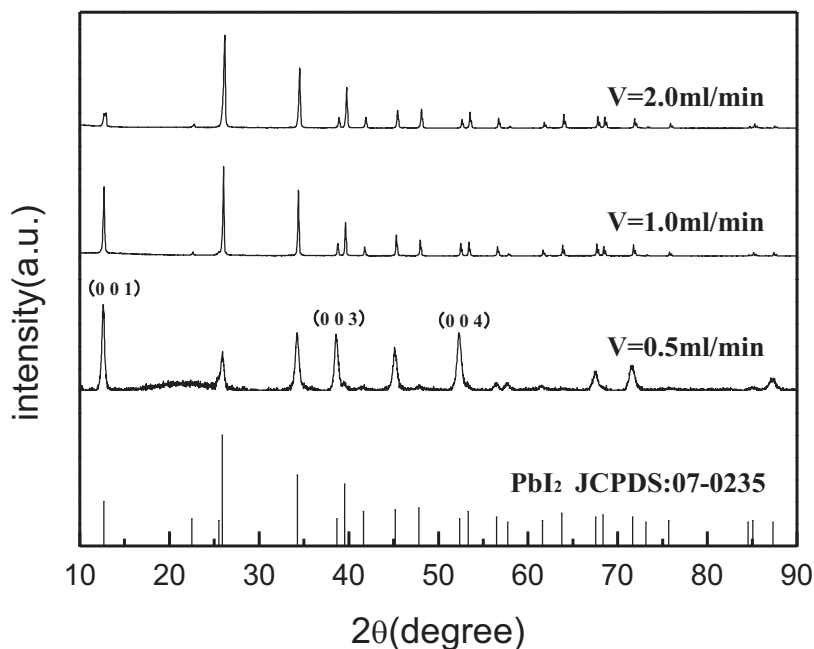
Fig. (4) shows the XRD results of lead iodide samples prepared under different lead ion concentrations. It can be seen that the solid prepared at lead ion concentrations of 0.01 M and 0.1 M is pure  $\text{PbI}_2$ . Interestingly, in the case of 0.01M  $\text{Pb}(\text{II})$  concentration, the main peaks of  $\text{PbI}_2$  at  $25.91^\circ$ ,  $34.27^\circ$ ,  $39.51^\circ$  did not increase sufficiently in size as was the case when using a 0.1M  $\text{Pb}(\text{II})$  solution, while the peaks at  $12.67^\circ$ ,  $38.67^\circ$ , and

$52.39^\circ$  became much stronger, indicating that some crystalline structures did not get enough precursor materials, which may be limited by the diffusion of lead and iodide ions. On the basis of the crystal growth theory, it can be deduced that in the case of very low  $\text{Pb}(\text{II})$ -concentrations, e.g. 0.01M lead ions, crystalline  $\text{PbI}_2$  particles have a strong ability to grow naturally according to their inherent crystalline habit in which the special

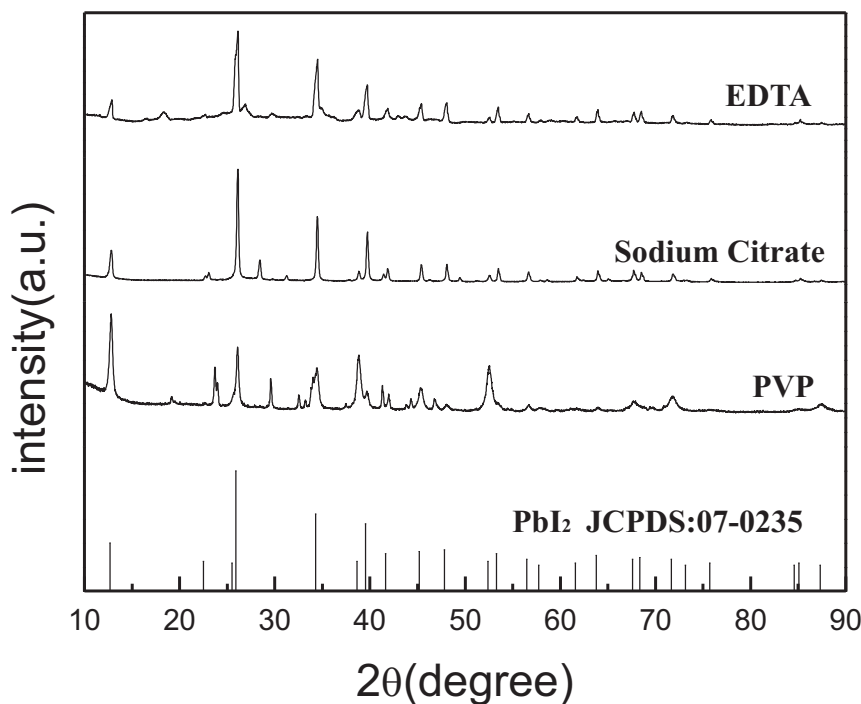
crystal facets grow preferentially, such as (001), (003) and (004), as shown in Fig. (4).

Fig. (5) shows the effect of feeding rates on the chemical compositions of the precipitated powder. The sample grows better as a crystal at a feed rate of 2.0 ml/min, indicating that at a higher feeding rate, the transportation rate of the precursors

of  $\text{PbI}_2$  crystalline nuclei growth is much larger, leading to a more sufficient growth of the crystals, which is quite identical to the variation behavior found in the case of low concentrations of lead ions. As shown in Fig. (4), the peaks at  $12.67^\circ$ ,  $38.67^\circ$  and  $52.39^\circ$  dominate at low concentrations, while the peaks at  $25.91^\circ$ ,  $34.27^\circ$  and  $39.51^\circ$  become the preferential ones in the case of high concentrations of lead ions.



**Fig. (5).** XRD patterns of the  $\text{PbI}_2$  powders synthesized at different feeding rates under the following experimental conditions:  $\text{pH}=4$ ,  $[\text{Pb(II)}]=0.03\text{ mol/L}$ ,  $t=70\text{ min}$ .



**Fig. (6).** XRD patterns of the  $\text{PbI}_2$  powders synthesized in the presence of different surfactants at all the concentrations of  $1\text{ g/L}$  under the following experimental conditions:  $\text{pH}=4$ ,  $[\text{Pb(II)}]=0.03\text{ mol/L}$ ,  $t=70\text{ min}$ ,  $V=1.0\text{ ml/min}$ .

Fig. (6) shows the diffraction peaks of the lead iodide powder prepared by adding different surfactants. It can be seen that the purity of the lead iodide sample produced with an addition of PVP (polyvinylpyrrolidone) as the surfactant is the lowest, while the purity of the samples with sodium citrate and EDTA as surfactants is similar, which may be due to the similar coordinative role of sodium citrate and EDTA. The slow release of lead ions makes the growth of crystalline nuclei possible according to the crystalline behavior of  $PbI_2$ , not leading to the random aggregation of tiny nuclei particles in the presence of PVP.

In order to investigate the effect of sodium citrate and EDTA on the formation of lead iodide, it is necessary to assess the concentration of the different lead species in the solution to explain the experimental results. Table 2 shows the thermodynamically calculated concentration of the species in the  $Pb^{2+}$ -I-Cit- $H_2O$  and  $Pb^{2+}$ -I-EDTA- $H_2O$  aqueous solutions. Fig. (7) shows the lead species in the solutions in the presence of citrate and EDTA, and it can be found that the introduction of chelating reagents will decrease the yields of the precipitated  $PbI_2$  solid, due to the competition for lead ions between the chelating reaction and the precipitation process. The stronger

the chelating affinity, the less the precipitation. This means that the yield of precipitated  $PbI_2$  in the presence of EDTA will be much smaller than that in the presence of citrate. However, considering the strict demands of solar cell fabrication, residual surfactants, such as citrate, EDTA and PVP may worsen the photoelectric properties of the cells. Thus, in the practical preparation process, additional surfactants are not recommended to be introduced in the precipitation system. For comparison, the effect of EDTA, PVP and citrate on the formation of  $PbI_2$  is worth investigating to determine the influence of the additive on the shape of precipitated lead iodide.

**Table 2. Thermodynamic data for calculated concentrations in the  $Pb^{2+}$ -I-Cit- $H_2O$  and  $Pb^{2+}$ -I-EDTA- $H_2O$  aqueous solutions.**

S. No.	Relation	Constant
1	$Pb^{2+}2I=PbI_2$	$9.80 \times 10^{-9}$
2	$Pb^{2+}+2OH=Pb(OH)_2$	$1.43 \times 10^{-15}$
3	$Pb^{2+}+C_6H_6O_7^{2-}=Pb(C_6H_6O_7)$	$10^{6.5}$
4	$Pb^{2+}+C_{10}H_{14}N_2O_8^{2-}=C_{10}H_{14}N_2PbO_8$	$10^{18.3}$

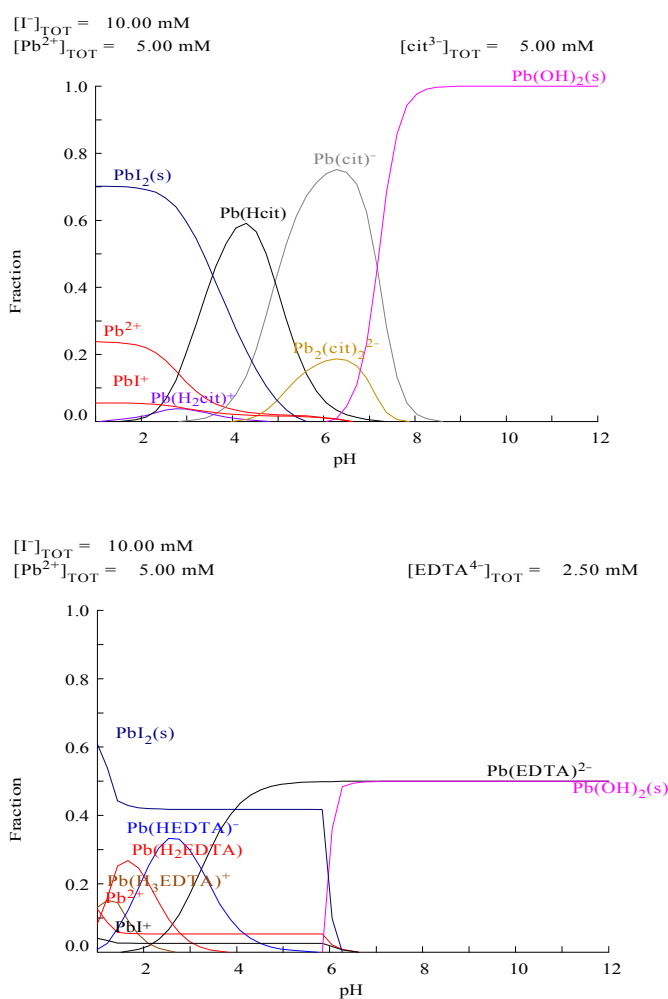


**Fig. (7).** Distribution species concentration of  $Pb^{2+}$  and I in the  $Pb^{2+}$ -I-Cit- $H_2O$  and  $Pb^{2+}$ -I-EDTA- $H_2O$  aqueous solutions.

### 3.2. SEM/EDS

Fig. (8) shows the morphology of lead iodide produced at different values of pH. It can be seen that there is not much difference between the samples obtained at pH=2 and pH=4, which are approximately hexagonal flakes with a size of about 10  $\mu\text{m}$ . The particles have good crystallinity. The energy spectrum results show that the sample is lead iodide. However, when the pH value rises to 6, the chemical composition of the precipitated sample can be found to change greatly. There is also a significant change in the morphology. Lead iodide particles do not precipitate in sheet-like hexagons, which seem like flocculated particles with larger blocks inside. Obviously, the chemical composition of the precipitates determines the morphology, where the chemical is affected by the solution pH, according to the preceding discussion.

As stated in the Weimarn rule [41 - 43], when the concentration of the lead ions is high, *e.g.* 0.1mol/L, the nucleation will dominate the precipitation process, leading to

the formation of very fine crystals, while in the case of dilute lead ions of a concentration of 0.01 mol/L, the growth of nuclei will become preferential to nucleation, producing larger particles. Fig. (9) illustrates the morphology of lead iodide prepared at different lead ion concentrations. We can observe that when the concentration is 0.01M, the shape of lead iodide is flake-like with a size larger than 10 $\mu\text{m}$ ; when the concentration is 0.1M, the particles having a size of about 5  $\mu\text{m}$  are closely packed with a sheet having a size of about 10  $\mu\text{m}$ . Fig. (10) shows the morphology of lead iodide at different feed rates. At a feeding rate of 0.5 mL/min., the surface of the sample is rough and the overall size is large. When the feeding rate is 2.0 mL/min., the surface of the sample is smooth, but the particle size varies from 5 $\mu\text{m}$  to 10  $\mu\text{m}$ . Fig. (11) shows the morphology of lead iodide samples after the addition of PVP, sodium citrate and EDTA. The sample with PVP had a rough surface and no regular shape, while the sample with sodium citrate had a small particle size, and the particle morphology of the sample with EDTA was a much fine flake-like shape.

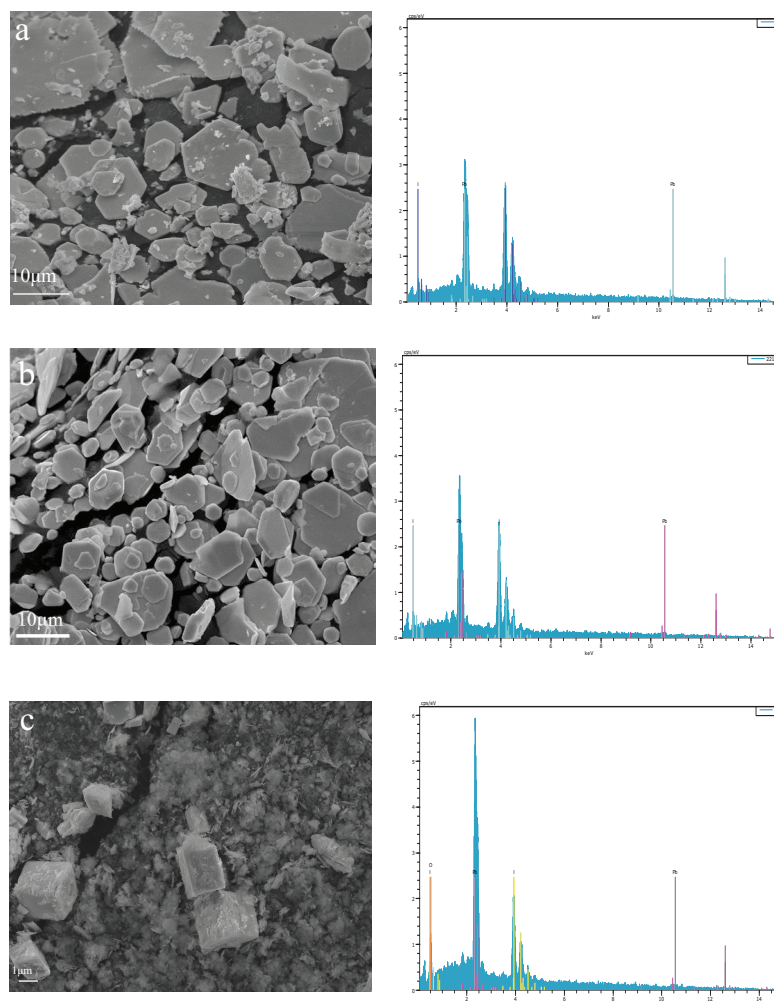


**Fig. (8).** SEM and EDS images of the  $\text{PbI}_2$  powders synthesized at different pH: pH=2 (a), pH=4 (b), pH=6 (c) under the following experimental conditions:  $[\text{Pb(II)}]=0.03\text{mol/L}$ ,  $t=70\text{min}$ ,  $V=1.0\text{ml/min}$ .

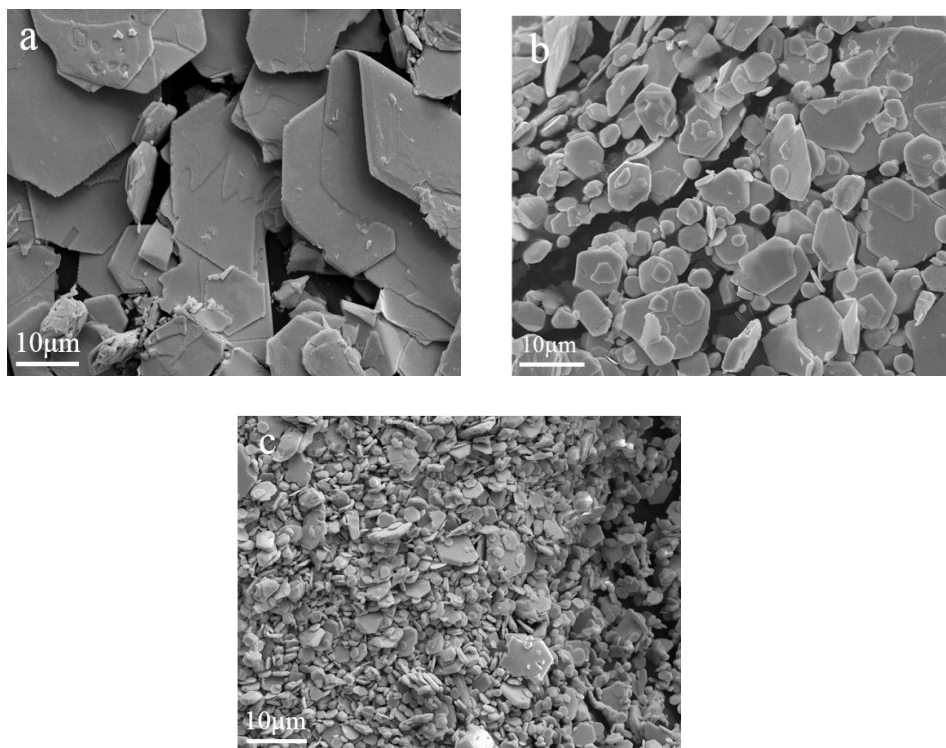


**Fig. (9).** SEM images of the  $PbI_2$  powders synthesized at different lead ion concentrations:  $[Pb(II)]=0.01\text{mol/L}$  (a),  $[Pb(II)]=0.03\text{mol/L}$  (b),  $[Pb(II)]=0.1\text{mol/L}$  (c).

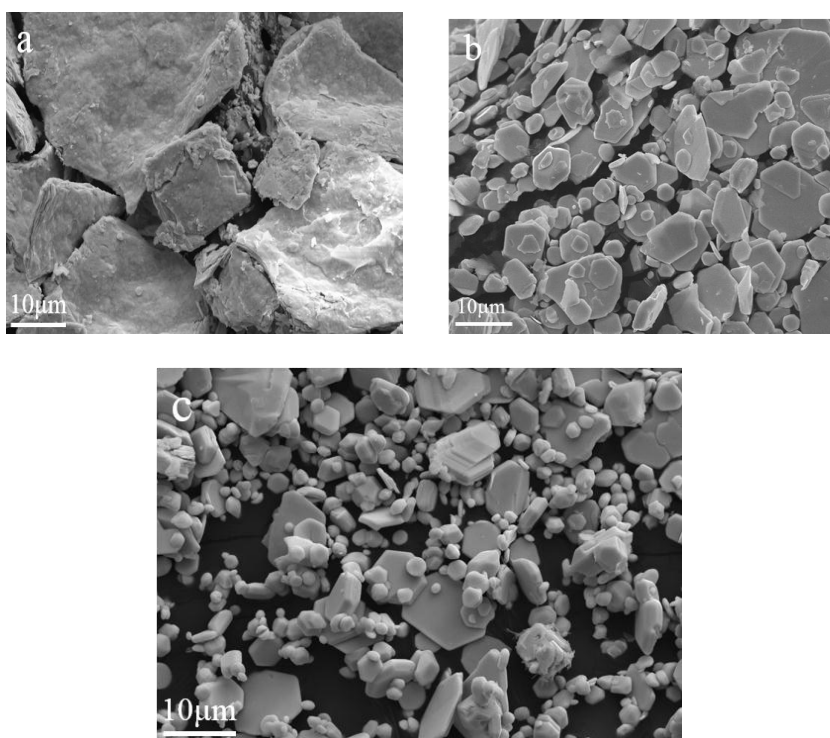


**Fig. (10).** SEM images of the  $PbI_2$  powders synthesized at different feeding rates:  $V=0.5\text{ml/min}$  (a),  $V=1.0\text{ml/min}$  (b),  $V=2.0\text{ml/min}$  (c) under the following experimental conditions:  $\text{pH}=4$ ,  $[Pb(II)]=0.03\text{mol/L}$ ,  $t=70\text{min}$ .

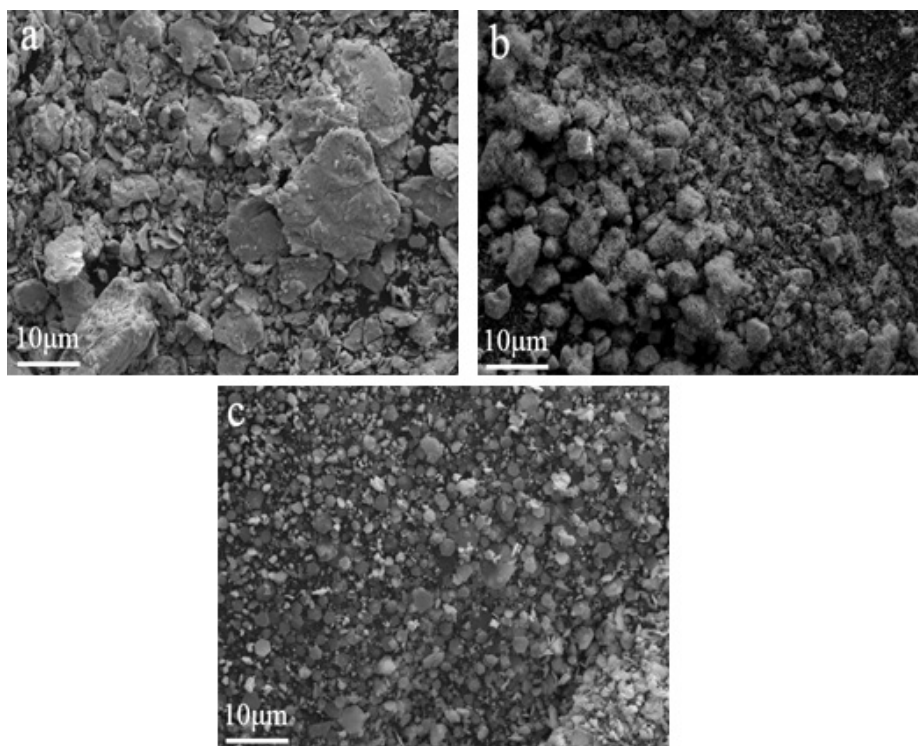


**Fig. (11).** SEM images of the  $\text{PbI}_2$  powders synthesized using different surfactants: 1g/L PVP (a), 1g/L sodium citrate (b), 1g/L EDTA (c) under the following experimental conditions: pH=4,  $[\text{Pb(II)}]=0.03\text{mol/L}$ ,  $t=70\text{min}$ ,  $V=1.0\text{ml/min}$ .

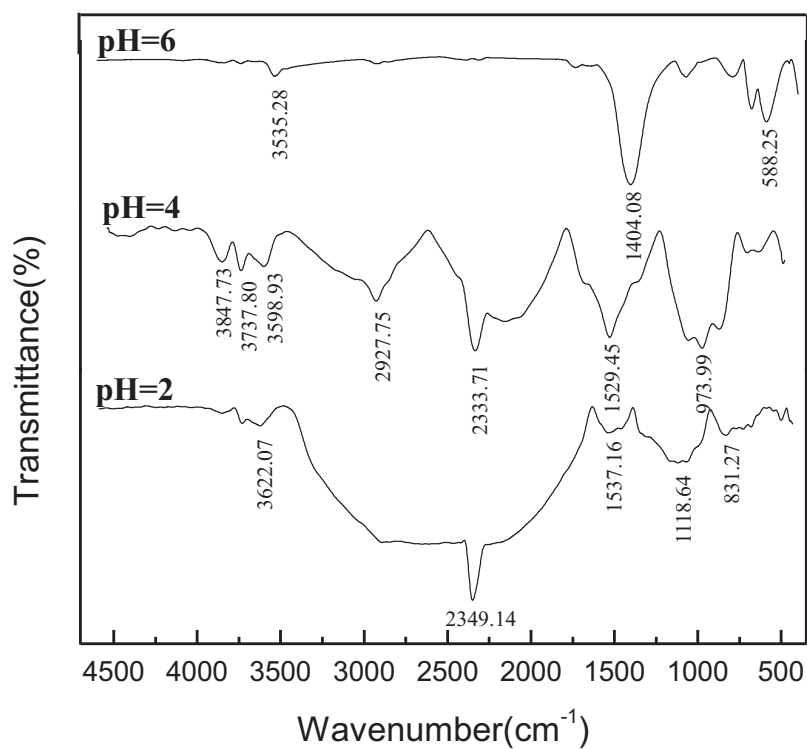


**Fig. (12).** FTIR absorption spectra of the  $\text{PbI}_2$  powders synthesized at different pH under the following experimental conditions:  $[\text{Pb(II)}]=0.03\text{mol/L}$ ,  $t=70\text{min}$ ,  $V=1.0\text{ml/min}$ .

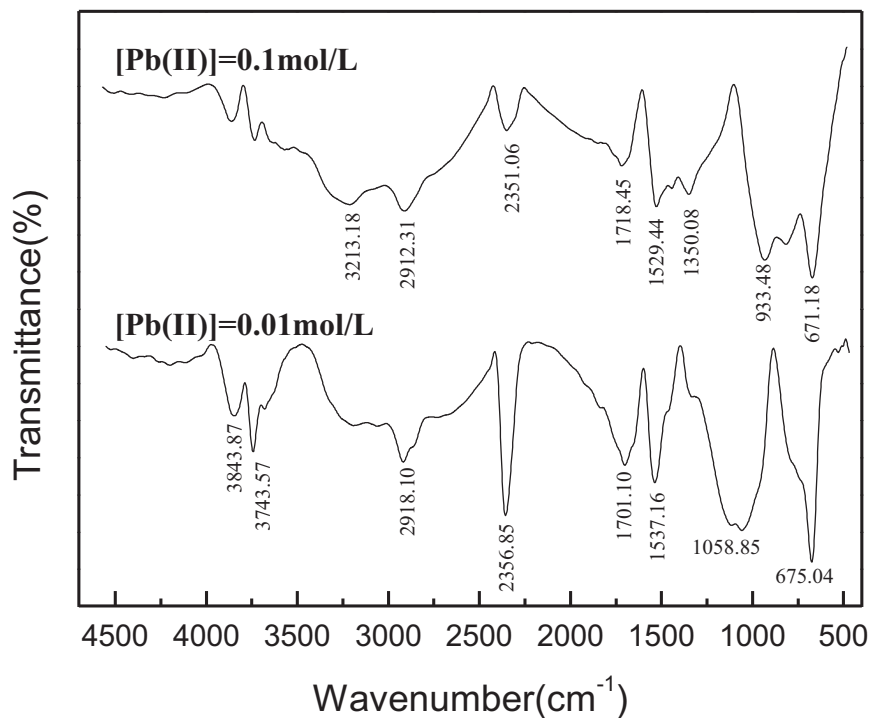


**Fig. (13).** FTIR absorption spectra of the  $PbI_2$  powders synthesized at different lead ion concentrations under the following experimental conditions:  $pH=4$ ,  $t=70min$ ,  $V=1.0ml/min$ .

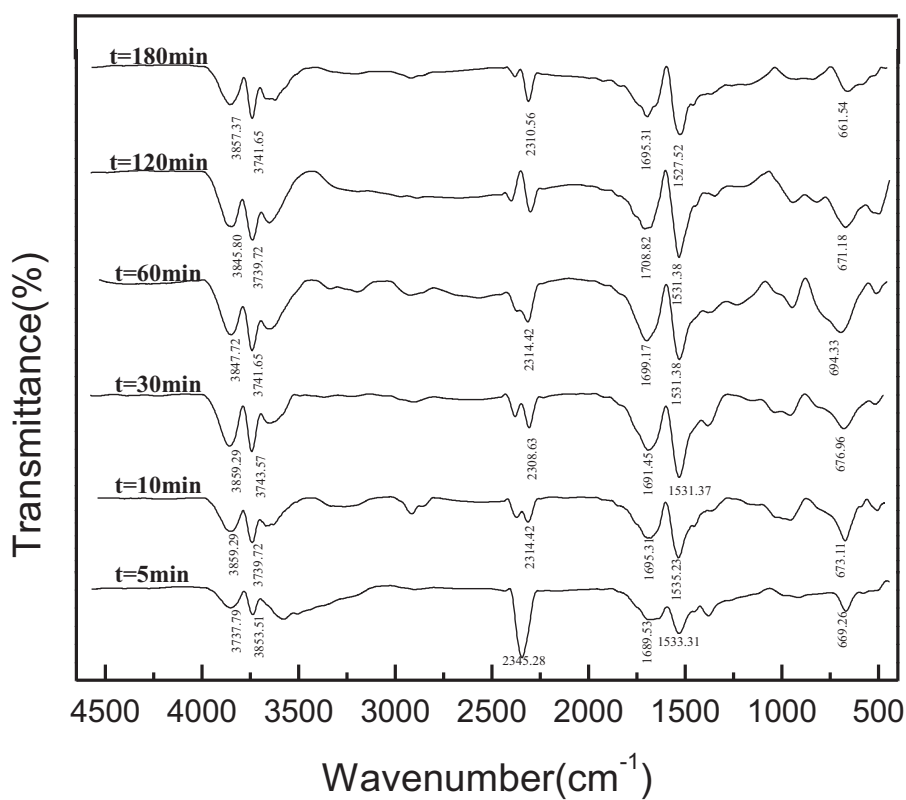


**Fig. (14).** FTIR absorption spectra of the  $PbI_2$  powders synthesized at different reaction times under the following experimental conditions:  $pH=4$ ,  $[Pb(II)]=0.03mol/L$ ,  $V=1.0ml/min$ .

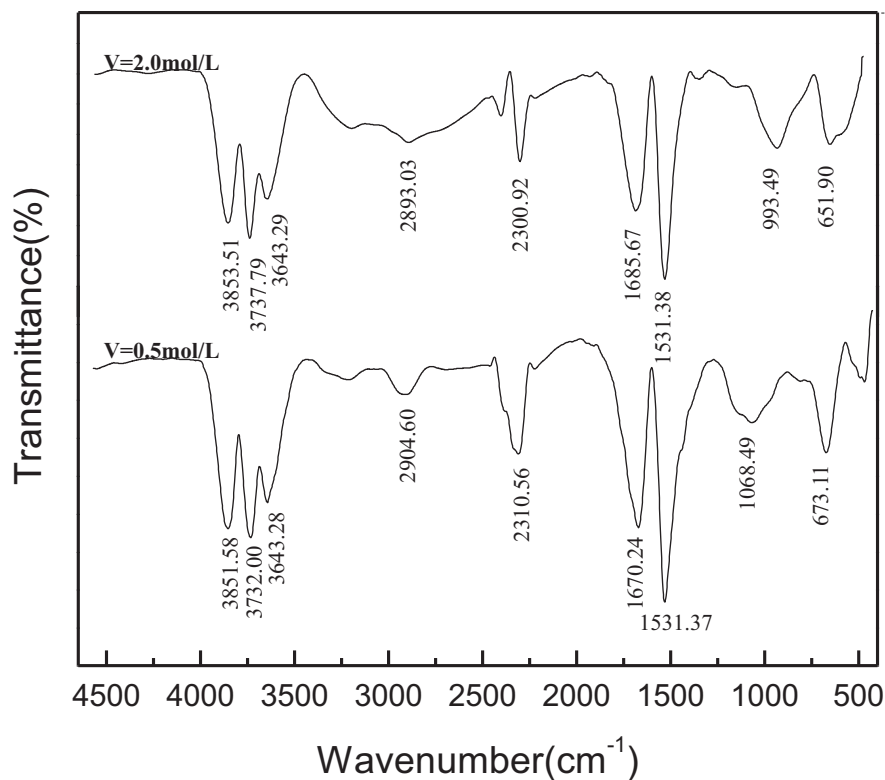


**Fig. (15).** FTIR absorption spectra of the  $PbI_2$  powders synthesized at different feeding rates under the following experimental conditions:  $pH=4$ ,  $[Pb(II)]=0.03\text{ mol/L}$ ,  $t=70\text{ min}$ .

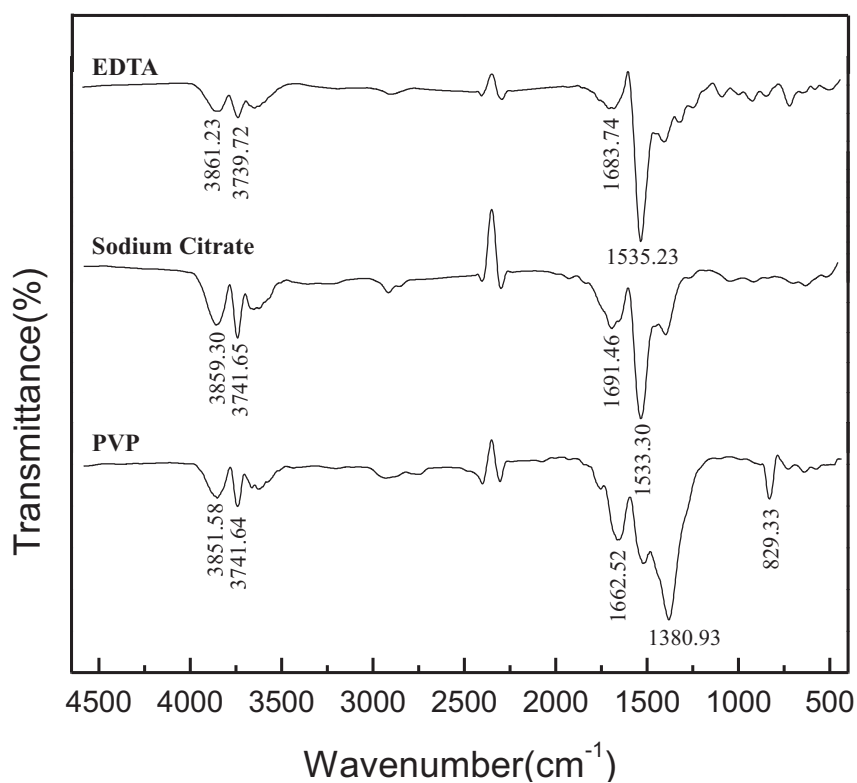


**Fig. (16).** FTIR absorption spectra of the  $PbI_2$  powders synthesized in the presence of different surfactants under the following experimental conditions:  $pH=4$ ,  $[Pb(II)]=0.03\text{ mol/L}$ ,  $t=70\text{ min}$ ,  $V=1.0\text{ ml/min}$ .

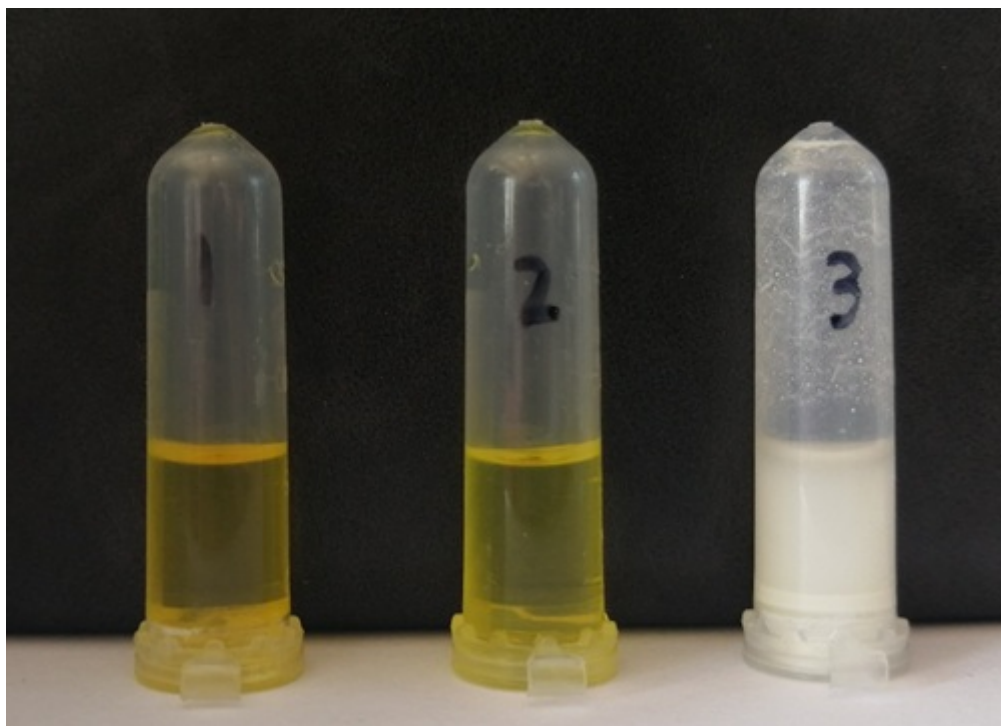


**Fig. (17).** Pictures to demonstrate the dissolving state of the  $PbI_2$  powders in DMF reagent synthesized under the following conditions:  $[Pb(II)]=0.03\text{mol/L}$ ,  $t=70\text{min}$ ,  $V=1.0\text{ml/min}$ ,  $\text{pH}=2$  (No.1),  $\text{pH}=4$  (No.2), and  $\text{pH}=6$  (No.3).

### 3.3. FTIR

As mentioned in the preceding section, from the X-ray diffraction results, we learned that all the samples prepared under acidic conditions were high-purity lead iodide. For further observation, the effect of synthesis parameters on the changes in the purity of lead iodide was analyzed by FT-IR spectroscopy. It can be seen from Fig. (12) that the change in pH has a great influence on the synthesis of lead iodide. When the pH is 6, the synthesized product is not lead iodide. The key to synthesizing high-purity lead iodide is to control the pH. It can be seen from Fig. (13) that the absorption peak decreases when the concentration of lead ions is increased. It can be seen from Fig. (14) that during the titration process, as the reaction time increases, the absorption peak near  $670\text{ cm}^{-1}$  of lead iodide gradually increases, and after the end of the mixed titration, the absorption peak gradually decreases. It can be seen from Fig. (15) that there is no obvious change in the respective absorption peaks of lead iodide, therefore, the purity has no significant relationship with the feeding rate. It can be seen in Fig. (16) that the absorption peaks appear at  $1380.93\text{ cm}^{-1}$  and  $829.33\text{ cm}^{-1}$  after the addition of PVP, indicating that PVP has an effect on the purity of lead iodide. There is no significant difference in the absorption peak between lead iodide added with sodium citrate and lead iodide added with EDTA, indicating that sodium citrate and EDTA will not affect the phase purity of lead iodide.

### 3.4. Solubility in DMF

To evaluate the solubility of the precipitated powder, which is an essential parameter that can preliminarily identify

the possibility of the precipitated particles to be used as a raw material for the fabrication of perovskite solar cell film, an attempt was made to dissolve the prepared  $PbI_2$  solids in DMF to form homogeneous clear solutions. This can be used to check the quality of  $PbI_2$ , as a conventional method.

0.5 gram of the sample, obtained at different pH (2, 4 and 6), was taken and mixed in 1 ml DMF solvent for 15 min at  $80^\circ\text{C}$ , and the mixtures were observed in regard to their color and turbidity. It can be seen in Fig. (17) that the powder samples precipitated at pH 2 and 4 were completely dissolved and formed transparent yellow solutions, while the sample formed at pH 6 gave a grey-white turbid suspension because of the insolubility in DMF of  $PbIOH$  that was obtained at pH 6. Evidently, the pH determines the phase and chemical compositions of the precipitated particles, and pure lead iodide can dissolve in DMF easily to form a homogeneous solution, which is good for further application in the fabrication of film coating for perovskite solar cells.

### CONCLUSION

A pH-controlled double jet precipitation process was designed to prepare lead iodide powders with high purity. Various parameters of precipitation were investigated for their influence on the chemical compositions and crystalline phases of the precipitated materials, as analyzed by XRD, SEM/EDS, and FTIR. All the results were used to identify the purity and morphology of the obtained lead iodide. It was found that lower concentrations of lead ions and feeding rates will cause the growth of nuclei to dominate the precipitation process and produce fine particles. Simultaneously, the growth rate of the

specific crystalline facets of  $\text{PbI}_2$  was also found to be strongly dependent on the concentration and feeding rate. Organic additives such as citrate, EDTA and PVP also have a drastic influence on the morphology of the precipitated particles. Therefore, the size and morphology of precipitated lead iodide can be tailored by controlling the above parameters. The suitable pH for the preparation of high-purity  $\text{PbI}_2$  was experimentally determined to be below 5.0, and a pH between 2.0 and 4.0 was recommended for the purity and production ratio in the real preparation process. The purity of lead iodide is the key factor in influencing its solubility in DMF, where the introduction of  $\text{PbIOH}$  to lead iodide as a contaminant during the precipitation process easily occurs at a pH above 5.0. Therefore, strict control of the pH below 5.0 is the key to assure the high purity of the precipitated lead iodide.

#### CONSENT FOR PUBLICATION

Not applicable.

#### CONFLICT OF INTEREST

The authors declare no conflict of interest, financial or otherwise.

#### ACKNOWLEDGEMENTS

Declared none.

#### REFERENCES

- [1] Liu, J.; Zhang, Y. Effect of temperature gradient on the growth of  $\text{PbI}_2$  crystal for nuclear radiation detectors. *B Chin. Ceram. Soc.*, **2016**, *35*(11), 3893-3897.
- [2] Zhang, J.; Song, T.; Zhang, Z. Layered ultrathin  $\text{PbI}_2$  single crystals for high sensitivity flexible photo detectors. *J. Mater. Chem. C Mater. Opt. Electron. Devices*, **2015**, *3*(17), 4402-4406. [http://dx.doi.org/10.1039/C4TC02712D]
- [3] Zhu, X.H.; Wei, Z.R.; Jin, Y.R. Growth and characterization of a  $\text{PbI}_2$  single crystal used for gamma ray detectors. *Cryst. Res. Technol.*, **2007**, *42*(5), 456-459. [http://dx.doi.org/10.1002/crat.200610847]
- [4] Liu, W.; Liu, Y.; Chen, L. Gel-incorporated  $\text{PbS}$  and  $\text{PbI}_2$  single-crystals. *Chin. Chem. Lett.*, **2015**, *26*(5), 504-508. [http://dx.doi.org/10.1016/j.ccl.2015.01.020]
- [5] Zhao, X. Research development of  $\text{PbI}_2$  single crystal growth and room-temperature nuclear radiation detectors. *Mater. Rev.*, **2011**, *25*(1), 80-83.
- [6] Novosad, S.S.; Novosad, I.S.; Matviishin, I.M. Luminescence and Photosensitivity of  $\text{PbI}_2$  Crystals. *Inorg. Mater.*, **2002**, *38*(10), 1058-1062. [http://dx.doi.org/10.1023/A:1020541724679]
- [7] Zhu, G.Q.; Mirabbos, H.; Liu, P. The effects of synthesis parameters on the formation of  $\text{PbI}_2$  particles under DTAB-assisted hydrothermal process. *Mater. Chem. Phys.*, **2011**, *131*(1-2), 64-71. [http://dx.doi.org/10.1016/j.matchemphys.2011.07.010]
- [8] Shkir, M.; Yahia, I.S.; Alfaify, S.; Abutalib, M.M.; Muhammad, S. Facile synthesis of lead iodide nanostructures by microwave irradiation technique and their structural, morphological, photoluminescence and dielectric studies. *J. Mol. Struct.*, **2016**, *1110*, 83-90. [http://dx.doi.org/10.1016/j.molstruc.2016.01.014]
- [9] Li, W.X.; Yang, J.; Jiang, Q. Electrochemical deposition of  $\text{PbI}_2$  for perovskite solar cells. *Sol. Energy*, **2018**, *159*, 300-305. [http://dx.doi.org/10.1016/j.solener.2017.10.077]
- [10] Street, R.A.; Ready, S.E.; Schuylenbergh, K.V. Comparison of  $\text{PbI}_2$  and  $\text{HgI}_2$  for direct detection active matrix x-ray image sensors. *J. Appl. Phys.*, **2002**, *91*(5), 3345-3355. [http://dx.doi.org/10.1063/1.1436298]
- [11] Liu, J Q; Liang, Z H; Xu, B Synthesis of  $\text{PbI}_2$  nanowires for high sensitivity photodetectors. *RSC Adv.*, **2016**, *6*(64), 59445-59449.
- [12] Liu, X.; Ha, S.T.; Zhang, Q.; de la Mata, M.; Magen, C.; Arbiol, J.; Sum, T.C.; Xiong, Q. Whispering gallery mode lasing from hexagonal shaped layered lead iodide crystals. *ACS Nano*, **2015**, *9*(1), 687-695. [http://dx.doi.org/10.1021/nn5061207] [PMID: 25562110]
- [13] Li, R.; Zhang, H.Y.; Zhang, M. Effect of  $\text{PbI}_2$  solution on air-preparation of perovskite solar cells for enhanced performance. *Appl. Surf. Sci.*, **2018**, *458*, 172-182. [http://dx.doi.org/10.1016/j.apsusc.2018.07.083]
- [14] Kim, H.S.; Lee, C.R.; Im, J.H.; Lee, K.B.; Moehl, T.; Marchioro, A.; Moon, S.J.; Humphry-Baker, R.; Yum, J.H.; Moser, J.E.; Grätzel, M.; Park, N.G. Lead iodide perovskite sensitized all-solid-state submicron thin film mesoscopic solar cell with efficiency exceeding 9%. *Sci. Rep.*, **2012**, *2*(8), 591. [http://dx.doi.org/10.1038/srep00591] [PMID: 22912919]
- [15] Cai, B.; Xing, Y.; Yang, Z. High performance hybrid solar cells sensitized by organolead halide perovskites. *Energy Environ. Sci.*, **2013**, *6*(5), 1480-1485. [http://dx.doi.org/10.1039/c3ee40343b]
- [16] Kong, W.M.; Li, G.H.; Liang, Q.B. Controllable deposition of regular lead iodide nanoplatelets and their photoluminescence at room temperature. *Physica E*, **2018**, *97*, 130-135. [http://dx.doi.org/10.1016/j.physe.2017.10.021]
- [17] Mitzi, D.B. Solution-processed inorganic semiconductors. *J. Mater. Chem.*, **2004**, *14*(15), 2355-2365. [http://dx.doi.org/10.1039/b403482a]
- [18] Wang, L.; Jia, D.Z.; Liu, L. Synthesis of surface-modified lead iodide nanorods by room temperature solid-state reaction. *Acta Chim. Sin.*, **2005**, *63*(6), 503-506.
- [19] Liang, Q.J.; Han, J.; Li, H.X. Uniform, high crystalline, (100) crystal orientated perovskite films without  $\text{PbI}_2$  residue by controlling the nanostructure of  $\text{PbI}_2$ . *Org. Electron.*, **2018**, *53*, 26-34. [http://dx.doi.org/10.1016/j.orgel.2017.10.037]
- [20] Zuo, L.; Gu, Z.; Ye, T.; Fu, W.; Wu, G.; Li, H.; Chen, H. Enhanced photovoltaic performance of  $\text{CH}_3\text{NH}_3\text{PbI}_3$  perovskite solar cells through interfacial engineering using self-assembling monolayer. *J. Am. Chem. Soc.*, **2015**, *137*(7), 2674-2679. [http://dx.doi.org/10.1021/ja512518r] [PMID: 25650811]
- [21] Qiu, L.; Deng, J.; Lu, X.; Yang, Z.; Peng, H. Integrating perovskite solar cells into a flexible fiber. *Angew. Chem. Int. Ed. Engl.*, **2014**, *53*(39), 10425-10428. [http://dx.doi.org/10.1002/anie.201404973] [PMID: 25047870]
- [22] Anaraki, E.H.; Kermanpur, A.; Steier, L. Highly efficient and stable planar perovskite solar cells by solution-processed tin oxide. *Energy Environ. Sci.*, **2016**, *9*, 3128-3134. [http://dx.doi.org/10.1039/C6EE02390H]
- [23] Shkir, M.; Yahia, I.S.; Ganesh, V. Facile hydrothermal-assisted synthesis of  $\text{Gd}^{3+}$  doped  $\text{PbI}_2$  nanostructures and their characterization. *Mater. Lett.*, **2016**, *176*, 135-138. [http://dx.doi.org/10.1016/j.matlet.2016.04.062]
- [24] Qin, H E; Jinglun, S; Dapeng, L I *In-situ* preparation of hexagonal lead iodide nanoflakes at room temperature. *J Xinyang Nomal Univ.*, **2018**, *31*, 100-103.
- [25] Shkir, M; Abbas, H Effect of thickness on the structural, optical and electrical properties of thermally evaporated  $\text{PbI}_2$  thin films. *J. Phys. Chem. Solids*, **2012**, *73*(11), 1309-1313. [http://dx.doi.org/10.1016/j.jpcs.2012.04.019]
- [26] Yu, Y.; Li, J.; Geng, D.; Wang, J.; Zhang, L.; Andrew, T.L.; Arnold, M.S.; Wang, X. Development of lead iodide perovskite solar cells using three-dimensional titanium dioxide nanowire architectures. *ACS Nano*, **2015**, *9*(1), 564-572. [http://dx.doi.org/10.1021/nn5058672] [PMID: 25549153]
- [27] Aricò, A.S.; Bruce, P.; Scrosati, B.; Tarascon, J.M.; van Schalkwijk, W. Nanostructured materials for advanced energy conversion and storage devices. *Nat. Mater.*, **2005**, *4*(5), 366-377. [http://dx.doi.org/10.1038/nmat1368] [PMID: 15867920]
- [28] Huang, B.; He, Q.; Fa, W. Rapid sonochemical preparation of shape-selective lead iodide. *Mater. Res. Bull.*, **2012**, *47*(9), 2599-2604. [http://dx.doi.org/10.1016/j.materresbull.2012.04.083]
- [29] Xiong, H.; Zhang, B.X.; Jia, W. Polymer PVP Additive for Improving Stability of Perovskite Solar Cells. *J. Inorg. Mater.*, **2019**, *34*(1), 96-102. [http://dx.doi.org/10.15541/jim20180172]
- [30] Stranks, S.D.; Eperon, G.E.; Grancini, G.; Menelaou, C.; Alcocer, M.J.; Leijtens, T.; Herz, L.M.; Petrozza, A.; Snaith, H.J. Electron-hole diffusion lengths exceeding 1 micrometer in an organometal trihalide perovskite absorber. *Science*, **2013**, *342*(6156), 341-344. [http://dx.doi.org/10.1126/science.1243982] [PMID: 24136964]

- [31] Liu, M.; Johnston, M.B.; Snaith, H.J. Efficient planar heterojunction perovskite solar cells by vapour deposition. *Nature*, **2013**, *501*(7467), 395-398. [http://dx.doi.org/10.1038/nature12509] [PMID: 24025775]
- [32] Wei, Q.B.; Qiao, Y.J.; Zhou, P. Fabrication of FA0.95 Cs0.05  $PbI_{3-x}$  Cl<sub>x</sub> perovskite solar cells using a single-step solution process *J. Funct. Mater.*, **2018**, *9*(49), 27-30.
- [33] Gao, X.Y.; Zhang, X.; Qin, X.Y. Thermal stability of the perovskite  $CH_3NH_3PbBr_3$  film prepared by using the two-step spin-coating method. *J. Zhengzhou Univ. (Nat. Sci. Ed.)*, **2018**, *50*(3), 100-104.
- [34] Tavakoli, M.M.; Gu, L.; Gao, Y.; Reckmeier, C.; He, J.; Rogach, A.L.; Yao, Y.; Fan, Z. Fabrication of efficient planar perovskite solar cells using a one-step chemical vapor deposition method. *Sci. Rep.*, **2015**, *5*, 14083. [http://dx.doi.org/10.1038/srep14083] [PMID: 26392200]
- [35] Chen, K.Q.; Du, X.; Lin, D.X. Progress in vapor evaporation synthesis of perovskite thin films and photovoltaic application. *J. Synthetic. Cryst.*, **2018**, *47*(9), 1823-1838.
- [36] Shi, Z.J.; Zhang, J H Preparation method for high-purity lead iodide film with controllable morphology. *CN patent CN107574409A* 2018.
- [37] Huang, Kai; Chen, Xing; Ma, Ruixin; Wang, Chengyan Method for preparing monodisperse high-purity lead iodide. *CN patent CN107739047A* 2018.
- [38] Tonn, J.; Danilewsky, A.N.; Croll, A. Czochralski growth of lead iodide single crystals: Investigations and comparison with the Bridgman method. *J. Cryst. Growth*, **2011**, *318*(1), 558-562. [http://dx.doi.org/10.1016/j.jcrysgro.2010.10.059]
- [39] Matuchova, M.; Zdansky, K.; Zavadil, J. Influence of doping and non-stoichiometry on the quality of lead iodide for use in X-ray detection. *J. Cryst. Growth*, **2010**, *312*(8), 1233-1239. [http://dx.doi.org/10.1016/j.jcrysgro.2009.12.034]
- [40] Sun, H.; Zhao, B.; Zhu, X. Laser-induced surface recrystallization of polycrystalline  $PbI_2$  thick films for X-ray detector application. *Appl. Surf. Sci.*, **2018**, *427*, 1146-1151. [http://dx.doi.org/10.1016/j.apsusc.2017.08.144]
- [41] Weimarn, V.P.P. The precipitation laws. *Chem. Rev.*, **1925**, *2*(2), 217-242. [http://dx.doi.org/10.1021/cr60006a002]
- [42] Guizhen, F.U. Research description of two kinds of nucleation of crystals theorys. *Shandong Ceramics*, **2013**, *36*(3), 18-22.
- [43] Ping, Y. Study of influence of cobalt oxalate precipitation process on cobalt powder size. *Cemented Carbide*, **2001**, *18*(1), 12-15.

© 2019 Huang *et al.*

This is an open access article distributed under the terms of the Creative Commons Attribution 4.0 International Public License (CC-BY 4.0), a copy of which is available at: (<https://creativecommons.org/licenses/by/4.0/legalcode>). This license permits unrestricted use, distribution, and reproduction in any medium, provided the original author and source are credited.